PHYSICAL REVIEW B **72**, 165428 (2005)

Elastic moduli of single-walled carbon nanotubes and their ropes

Shuchi Gupta, K. Dharamvir, and V. K. Jindal*,†
Department of Physics, Panjab University, Chandigarh-160014, India

(Received 14 June 2005; revised manuscript received 3 August 2005; published 27 October 2005)

We report the results of a model calculation for studying the effects of pressure on a bunch of carbon nanotubes as well as individual nanotubes. Carbon nanotubes are extremely rigid in the axial direction. At pressures that we work with, the deformation in the axial direction comes out to be negligibly small in comparison to that in the transverse direction. We use the six-exponential and Brenner potentials to account for inter- and intratube interactions, respectively. Using second derivatives of potential, Young's modulus for single-walled armchair, zigzag and chiral tubes of different radii have been calculated. The values found by us in this simple model turn out to be in good agreement with other theoretical and experimental values. The strain dependence of Young's modulus has also been studied. We have also calculated the Poisson ratio and shear modulus of various single-walled nanotubes. We find that hydrostatic pressure is an ideal probe to study the radial deformations of the nanotubes. The nanotubes are considered to be flexible, identified by a flattening of cylinders under pressure through a parameter *f*. We calculate the total energy of the bunches having faceted tubes. The free energy thus calculated enables us to calculate phase changes at various pressures. From our calculations, we find the phase transformation to occur at about 5 GPa. Young's modulus of nanoropes has also been calculated at various pressures and at the phase transition we obtain a discontinuity in the curve. A much simplified form of the Brenner potential has been suggested and results are compared with those obtained from original form of Brenner potential.

DOI: 10.1103/PhysRevB.72.165428 PACS number(s): 61.46.+w

I. INTRODUCTION

Carbon nanotubes (CNTs) have hogged immense attention from the scientific community ever since their discovery. Their high aspect ratio, large tensile strength, the ability to exist in either metallic or semiconducting forms, and extreme flexibility make them promising candidates as high strength fibers and various novel nanometer scale electronic and mechanical devices. These nanotubes, which are rolled up sheets of graphite, exist in single- as well as multiwalled forms, called single-walled nanotubes (SWNTs) and multiwalled nanotubes (MWNTs), respectively. It has been found that the tensile strength of CNTs might exceed that of other known fibers because of the inherent strength of the carbon–carbon bond. A good deal of experimental and theoretical work has already been done to quantify the strength of nanotubes, by analyzing their elastic properties, which has been one of the most hotly disputed areas of nanotube study in recent years. The results of various studies over the years have shown a large variation in the value reported for Young's modulus, ranging from 0.6 TPa–5.0 TPa. In the rest of this section, we summarize the results of existing experiments and calculations.

In 1996, researchers at Nippon Electric Company in Princeton and the University of Illinois measured the average modulus to be 1.8 TPa.[1] Using a vibrating beam model, the first experimental measurements of Young's modulus of MWNTs were given by Treacy *et al.*[2] The results ranged from 0.40 to 4.15 TPa with a mean value of 1.8 TPa and an uncertainty of 1.4 TPa. A similar study (same method) on SWNTs by Krishnan *et al.*[3] found an average modulus of about 1.3−0.4/+0.6 TPa for 27 SWNTs. Wong *et al.*[4] measured the bending force and found Young's modulus of 1.28±0.59 TPa for MWNTs using atomic force microscopy (AFM). Forró *et al.*[5] noted that their modulus measurements of MWNTs in 1999 (using AFM) did not strongly depend on the diameter. Instead, they argued that the Young's modulus of MWNTs correlates to the amount of disorder in the nanotube walls. However, their evidence showed that the value for SWNTs does in fact depend on diameter and an individual tube had a modulus of about 1 TPa.

In 1997, Gao *et al.*[6] calculated Young's modulus to five decimal places. They considered three types of SWNTs and showed the values were dependent on the chiral vector. In 1999, Hernández and Rubio[7] showed, using tight-binding calculations, that the Young's modulus was dependent on the size of the SWNT. Tejima *et al.*,[8] using tight-binding molecular dynamics (MD) method and *ab initio* density functional theory, confirmed that nanotubes are extremely rigid in axial direction and the Young's modulus of the CNT is 1.06 TPa. The previous evidence would lead us to assume that the diameter and shape of the nanotube was the determining factor for its elastic modulus. However, Zhou *et al.*,[9] from electronic band theory, calculated its value to be about 5.0 TPa and that too independent of size and helicity of the tubes. Sears and Batra,[10] from molecular mechanics simulations of axial deformations of a SWNT, found that Young's modulus of an equivalent continuum tube made of a linear elastic isotropic material varies from 2.3 to 2.6 TPa and that the wrapping indices have a very little effect on the values. The controversy into the value of the modulus is, to a large extent, due to the authors' interpretation of the thickness of the walls of the nanotube.

A large variety of experiments and simulations have been carried out to estimate the mechanical moduli of CNTs. However, there are still no experimentally measured values of the shear modulus and Poisson ratio of CNTs available. Theoretical calculations are also very few. Yu *et al.*,[11] using

MD simulations, showed that the shear modulus of a CNT increases as the radius of the CNT enlarges, its value changes from 370 to 500 GPa and the shear modulus of a zigzag CNT is higher than that of an armchair CNT. Papadakis *et al.*[12] reported on the characterization of nanometer-scale resonators in which each device incorporates a MWNT as a torsional spring. Popov *et al.*[13] derived an analytical expression for the Youngs and shear moduli of CNTs based on lattice dynamics model. An extensive study of various elastic constants of CNTs, Youngs modulus, shear modulus, and Poisson ratio have been done by Lu[14] using an empirical pair potential. The empirical Tersoff–Brenner[15,16] potential has been used to model the interatomic forces.

Not only the deformations in the axial direction, but the behavior of the nanotube ropes under pressure along the radial direction, remain a topic of interest. Since the deformation of the cross section of the tube may affect various properties, it is of prime importance to study the behavior of SWNT bundles under pressure. There exists various theoretical and experimental evidence available in literature, indicating the pressure driven transformations in SWNTs. Chesnokov *et al.*[17] conducted the experiment up to a pressure of about 27 kbar and observed a large and reversible volume loss of the SWNT bundles. Several Raman spectroscopy studies have also been reported; e.g., Venkateswaran *et al.*[18] made investigations on the pressure dependence of the Raman active radial and tangential breathing modes of SWNT bundles and attributed the disappearance of radial mode intensity beyond 1.5 GPa to the faceting of nanotubes under pressure. Peters *et al.*[19] studied Raman shifts and reported a structural phase transition at a pressure of about 1.7 GPa. Recent measurements by Tang *et al.*[20] suggest that the tubes of diameter of about 14 Å may be slightly polygonized even at zero pressure, although this polygonization is more prominent for higher pressures and obtained a structural distortion at about 1.5 GPa, which is reversible up to a pressure of 4 GPa. Lopez *et al.*[21] observed the faceting of tubes of about 17 Å diameter from high-resolution transmission electron microscopy image. They also did MD simulations and found that the equilibrium configuration of the lattice corresponds to circular tubes; however, the lattice of faceted tubes is very close in energy. Rols[22] performed neutron diffraction studies up to 50 kbar and found that shape deformation dominates the compression process around 20 kbar pressure. However, x-ray studies conducted by Sharma *et al.*[23] showed the vanishing of the diffraction line thus indicating a phase transition ~10 GPa, which is not related to uniform flattening and/or uniform faceting of tubes but is due to loss of triangular lattice and this lattice reappears on unloading of pressure from ~13 GPa. Karmakar *et al.*,[24] using *in situ* x-ray diffraction and Raman scattering techniques, studied the behavior of SWNTs bundles under nonhydrostatic pressures. It was seen that the diffraction line corresponding to the two-dimensional triangular lattice in the bundles is not reversible for pressures beyond 5 GPa, in sharp contrast to earlier results under hydrostatic pressure conditions.

Therefore, a complete understanding of these pressure dependent transitions is still required. In this paper, we report calculations showing the reversible deformation of tubes from the circular to hexagonal cross section with an increase in pressure. We have made an effort to study the mechanical characteristics of SWNTs under axial strain and torsion in this paper. Young's modulus, shear modulus, and Poisson ratio of a series of nanotubes with different chiral and achiral geometries have been calculated. We have also calculated the Young's modulus of the bundle having deformed (or faceted) tubes. The algebraic expressions to obtain energy and elastic constants are also obtained.

In this paper, we have a given good qualitative picture to understand the pressure dependent tube deformations through a simple model. Though as we have already discussed, many other authors have also calculated Young's modulus, shear modulus, and Poisson ratio. But since we want to study the radial deformations of the nanotubes using hydrostatic pressures, it is useful to study these axial deformations, also. In addition to this, we have calculated the strain dependence of Young's modulus of SWNTs and pressure dependence of Young's modulus of nanoropes, also. The Brenner potential, especially the second term—which looks formidable to be handled algebraically—has been cast into a much simplified convenient form with certain approximations. Using this form, various quantities can be calculated analytically by just substituting the values in simple formulae. The potentials used are C—C interactions of the Brenner–Tersoff type for intramolecular and six-exponential for intermolecular interactions.

II. MODEL AND CALCULATIONS

The interaction between two carbon atoms on the same tube is modeled by an effective short-range potential of Tersoff–Brenner form. The potential energy between the atoms i and j on the same tube separated by a distance r_{ij} is of the form:

$$U(r_{ij}) = f_c(r_{ij})[Ae^{-\lambda_1 r_{ij}} - b_{ij}Be^{-\lambda_2 r_{ij}}], \tag{1}$$

where f_c is a cutoff function which is simply taken as:

$$f_c(r) = \begin{cases} 1, & r < (s-D), \\ \frac{1}{2} - \frac{1}{2}\sin\left[\frac{1}{2}\pi(r-s)/D\right], & (s-D) < r < (s+D), \\ 0, & r > (s+D). \end{cases} \tag{1a}$$

This form of cutoff, which goes from 1 to 0 in a small range, from $r=1.8$ Å to $r=2.1$ Å, and ensures that the potential applies only to those atoms which lie within a distance of 2.1 Å from each other, is continuous, and has a derivative for all r. s and D are both the potential parameters which are tabulated below in Table I. s is chosen to include only the first-neighbor shell. The function b_{ij} is an algebraic expression involving several parameters. It implicitly includes the bond order and depends on local atomic environment. All deviations from a simple pair potential are ascribed to the dependence of b_{ij} upon the local atomic environment. Specifically, the bonding strength b_{ij} for the pair ij should be a monotonically decreasing function of the coordination of atoms i and j. b_{ij} has the following form:

TABLE I. The short-range potential parameters.

	A (eV)	B (eV)	λ_1 (Å^{-1})	λ_2 (Å^{-1})	s (Å)	D (Å)	β (10^{-7})	n	c (10^4)	d	h
Brenner–Tersoff	1393.6	346.7	3.4879	2.2119	1.95	.15	1.5724	.72751	3.8049	4.3484	−.57058
Ours	1380	349.4	3.5679	2.2724	1.95	.15	1.5724	.72751	3.8049	4.3484	−.57058

$$b_{ij} = \frac{1}{(1+\beta^n \varsigma_{ij}^n)^{1/2n}}, \tag{1b}$$

where

$$\varsigma_{ij} = \sum_k f_c(r_{ij}) g(\theta_{ijk}) \exp[\lambda_3^3 (r_{ij} - r_{ik})^3] \tag{1c}$$

with

$$g(\theta) = 1 + \frac{c^2}{d^2} - \frac{c^2}{[d^2 + (h - \cos\theta)^2]}. \tag{1d}$$

In Eq. (1c), the summation over k runs over neighbors of i leaving out j; and θ_{ijk} is the angle between bonds ij and ik.

Most of the parameters used in this potential are taken to be the same as those given by Tersoff[16] except for a few, A, B, λ_1, and λ_2, which are modified by us in order to get a better fit to the bond length and cohesive energy of graphite. These parameters are tabulated in Table I. λ_3 is taken to be equal to 0.

Upon rearranging the terms in Eq. (1), the Brenner potential can be written in a much simpler form, with a few approximations; as shown in Appendix A.

A. Bending energy of a single-walled nanotube

Each tube is an elastic sheet bent into a cylindrical form. Upon bending the graphene sheet to form a tube, the angles between neighboring bonds change. So the bonding strength b_{ij} also changes. Using the Tersoff–Brenner potential with modified parameters, bending energy for SWNT of the "armchair" variety with various radii R are calculated (shown in Table II). We consider a rolled up graphene sheet consisting of a certain number of hexagonal rings along its circumference. The coordinates of C atoms on such a cylinder are known (they are generated using those of graphene). The total bond energy for this configuration, using the Brenner potential [Eq. (1)] is calculated. Before folding the graphene sheet, its energy is minimized. But when it is folded to form a tube, it might happen that the tube is not in a minimized configuration and, therefore, the coordinates are adjusted a little until the total energy obtained reaches a minimum value. This is repeated for various diameters of tube. We find that these calculations are in close agreement with the Quantum Molecular Dynamical calculations performed by Adams *et al.*[25] Bending energy, E_{bending}, is defined as the difference in the bond energies of a tube compared to the total bond energy of same area of a plane sheet of graphene.

TABLE II. Bending energy for tubes of different radii.

Radius (Å)	Energy per atom (eV)	E(QMD)[a]
3.39	.183	.182
4.07	.126	.126
5.43	.070	.071
6.78	.044	.045

[a] See Ref. 12.

Figure 1 is a plot of energy per unit area of tube surface (due to bending) as a function of the inverse square radius of the tube. It follows that when a piece of graphene sheet is bent to form part of a cylinder of radius r, the energy spent is proportional to $1/r$. Thus, the graph between the bending energy per unit area and $1/r^2$ is a straight line as shown. Expressing the total bending energy associated with the tube in terms of a constant c_o,

$$E_{\text{bending}} = \frac{\pi c_o L}{r}, \tag{2}$$

where L is the length of the tube and we have calculated the value of elastic bending constant, c_o, for armchair, zigzag, and chiral tubes, tabulated in Table III.

III. EFFECT OF THE PRESSURE APPLIED AXIALLY ON THE TUBE

By applying the pressure along the tube axis, various elastic moduli have been calculated. The estimation of these elastic moduli requires the knowledge of the "wall thickness" of the tubes if we consider it to be a hollow cylinder. Some authors take it to be equal to .66 Å (Ref. 26) and some

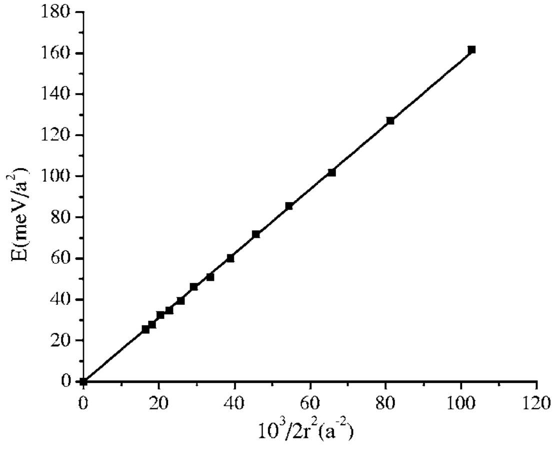

FIG. 1. Energy per unit area as a function of radius of curvature for (n,n) tubes (a=lattice constant of the graphene sheet=2.46 Å).

TABLE III. Elastic bending constant for different tubes.

Tube	c_0 (eV)
(n,n)	1.54
$(n,0)$	1.64
$(2n,n)$	1.69

consider it to be 3.4 Å,[13,14] equal to the adjacent layer separation in graphite. We too have adopted the conventional thickness of 3.4 Å.

A. Young's modulus

We first obtain the position coordinates of carbon atoms on the surface of a nanotube of given chirality (n,m) (Ref. 27) and length (taken to be ~50 Å in this case). The coordinates are first generated by taking into consideration the geometry and chirality of a given nanotube and then the tube is allowed to relax under the given potential until we get the minimized stable configuration. We then consider the same tube under longitudinal stress. This stress is simulated by either taking a slightly elongated (tensile stress) or shortened (compressive stress) tube. The coordinates of the rest of the atoms of the tube are varied till minimum energy is obtained. The potential energy (PE) curve thus obtained (a sample is shown in Fig. 2).

The force which produces a certain extension, say $l-l_0$ (or Δl), is obtained by the first derivative at l, since

$$F=-\frac{\partial U}{\partial l}. \tag{3}$$

The standard expression for Young's modulus is

$$Y=\frac{F/a}{\Delta l/l_0}, \tag{4}$$

where l_0 is the length of the tube and a is the cross-sectional area.

Since, around the minimum,

$$U=k(\Delta l)^2, \tag{5}$$

where k is a constant given by $k=\frac{1}{2}\partial^2U/\partial l^2|_0$, we obtain

$$Y=\left(\frac{l}{a}\frac{\partial^2U}{\partial l^2}\right)_0. \tag{6}$$

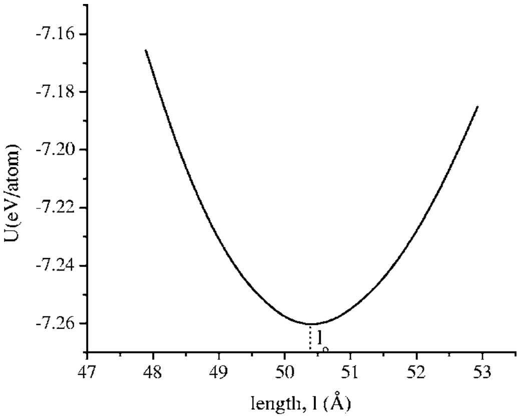

FIG. 2. PE curve for a (10,10) tube.

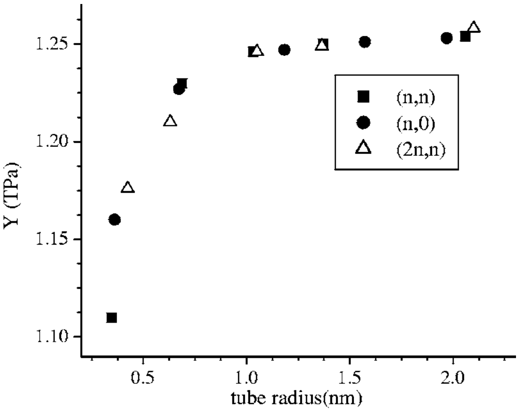

FIG. 3. Young's modulus for different tubes.

This quantity [right-hand side (rhs) of Eq. (6)] is plotted in Fig. 3. In this figure, calculations are presented for various armchair, zigzag, and chiral tubes. Some of these values are presented in Table IV for comparison. These calculations for Youngs modulus of SWNTs match quite accurately (within a few percent) the previously done work.

From Fig. 3, we find that as the radius of the tubes increases, Young's modulus is approaching a constant value, and for large diameters the value becomes equal to that of graphene sheet.

By increasing the axial strain, i.e., by further compressing or elongating the tubes, we again minimize the structures and get a new value of Young's modulus, Y at enhanced positive (tensile) or negative (compressive) stress values. We have done this calculation for a number of tubes, with different diameters and chiralities [one such case, for (10,10) tube is shown in Fig. 4]. Variation in the value of Y is due to anharmonicity, as can be seen as follows.

If instead of Eq. (5), we take a few more terms in the expansion of energy, then it becomes,

$$U-U_o=k(\Delta l)^2+p(\Delta l)^3+r(\Delta l)^4. \tag{7}$$

Parallel to Eq. (6), the expression for Young's modulus of a tube, already stretched by an amount Δl, is given by

$$Y=\left.\frac{l+\Delta l}{a}\frac{\partial^2U}{\partial l^2}\right|_{\Delta l},$$

which from Eq. (7) yields

$$Y\approx\frac{2l}{a}[k+3p\Delta l+6r(\Delta l)^2]. \tag{8}$$

On fitting the curve in Fig. 2 to the form in Eq. (7), we get

$$k=0.01325\ \text{eV/Å}^2,\quad p=-0.00063\ \text{eV/Å}^3,\quad \text{and}$$

$$r=2\times10^{-5}\ \text{eV/Å}^4. \tag{9}$$

From Eq. (8), using the values of coefficients from Eq. (9), we get the curve shown in Figs. 4(a) and 4(b), showing variation of Young's modulus with axial strain and as a func-

TABLE IV. Elastic moduli for some of the tubes.

	Tube	Radius (nm)	Y (TPa)		ν		G (GPa)	
			Present	Ref. 7	Present	Ref. 28	Present	Ref. 11
armchair	(5,5)	0.346	1.11	1.22 ((6,6))	0.145	.14	265.60	
	(10,10)	0.6878	1.23	1.24	0.148	.16	344.30	370
	(15,15)	1.032	1.246	1.25			362.10	
	(20,20)	1.371	1.25				369.30	
	(30,30)	2.059	1.254					
zigzag	(9,0)	0.361	1.16	1.22 ((10,0))	0.132	.19 (10,0)	303.41	
	(17,0)	0.673	1.227	1.26 ((20,0))	0.151		355.75	375
	(30,0)	1.183	1.247				371.07	
	(40,0)	1.573	1.251				374.20	
	(50,0)	1.969	1.253					
chiral	(8,4)	0.420	1.176		0.145	.18	176.41	
	(12,6)	0.630	1.20		0.147		302.41	
	(20,10)	1.050	1.246				350.99	
	(26,13)	1.365	1.249				361.49	
	(40,20)	2.1	1.258					

tion of stress. From Fig. 4, we find that it is easier to elongate the tube than to compress it as compressive stresses, the Young's modulus increases, and at tensile stresses, its value decrease as compared to the value at zero stress.

B. Shear modulus

Next, a twist is applied to the tube of a given chirality and diameter, keeping one of its ends fixed. The total torsion that has to be given to the tube has been distributed equally along the whole length of the tube, and again the coordinates of the tube in minimum energy configuration are obtained (see Fig. 5). Based on the theory of elasticity, shear modulus is given by (Appendix B)

$$G = \frac{Tl_o}{\theta J(t)}, \tag{10}$$

where T, l_o, and $J(t)$ stand for the torque acting at the end of the SWNT, the length of the tube, the total torsion angle that is applied to the tube, and the cross-sectional polar moment of inertia of the SWNT, respectively. The polar inertia $J(t)$ is a function of wall thickness and for a SWNT with radius r_o and wall thickness t, is given by (Appendix B)

$$J(t) = \frac{\pi}{2}\left[\left(r_o + \frac{t}{2}\right)^4 - \left(r_o - \frac{t}{2}\right)^4\right]. \tag{11}$$

Using Eq. (11), the shear modulus related to the tubes having different diameters and chiralities have been obtained and some of these are tabulated in Table IV. It is observed that shear modulus increases upon enlarging the tube diameter and its value for the zigzag tube is a little higher than that for armchair tube. This is in accordance with Yu *et al.*[11]

C. Poisson ratio

Another mechanical property of interest is the Poisson ratio, ν, which is given by the variation of the radius of SWNT resulting from applying the axial strain on the tube.

$$\nu = -\frac{\text{lateral strain}}{\text{longitudinal strain}} = -\frac{\Delta r/r_o}{\Delta l/l_o} = -\frac{r_s - r_o/r_o}{\varepsilon}, \tag{12}$$

where $\varepsilon = \Delta l/l_0$=axial strain, r_s is the radius of the strained tube, and r_o is the radius of the unstrained tube.

The longitudinal stress is applied on the tube by elongating or compressing it, and the coordinates of the atoms on the tube are allowed to relax until a stable configuration with minimum energy is obtained. The radius of this minimized configuration gives us r_s corresponding to that particular axial strain. We have calculated ν for the tubes under study. Poisson ratio for various tubes are tabulated in Table IV. This value is considerably smaller than the value $\nu = .28$ given by Lu[14] but closer to the value $\nu = .19$ obtained by Yakobson *et al.*[26] using Tersoff–Brenner potential. The corresponding magnitude along the basal plane in graphite is $\nu = .16$.[28,29]

IV. SIMPLIFIED BRENNER POTENTIAL

Brenner potential [Eq. (1)] can be re-written, with certain approximations, as [details to derive this expression are given in Appendix A]

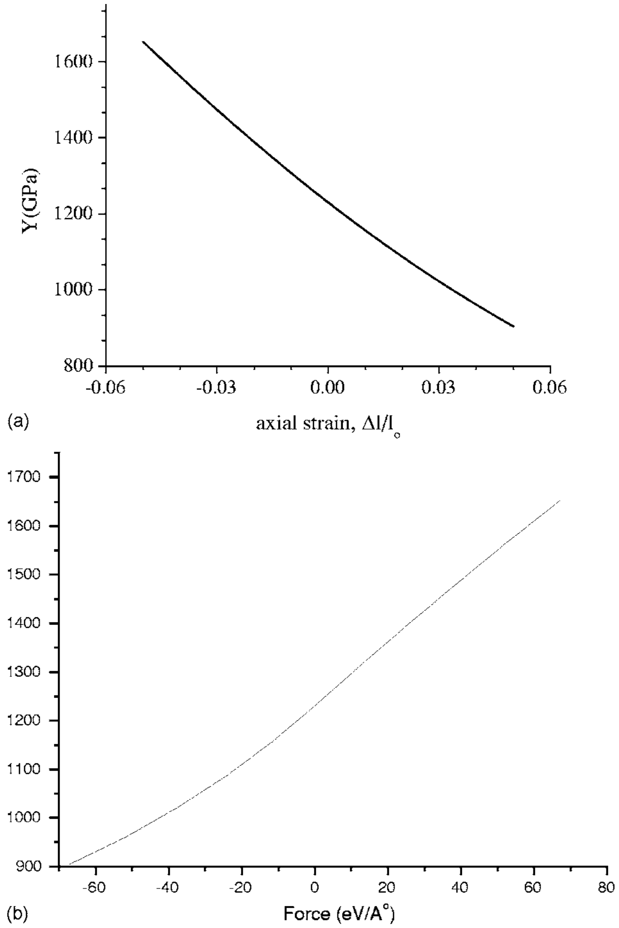

FIG. 4. (a) Young's modulus for a (10, 10) tube as a function of axial strain. (b) Young's modulus for a (10, 10) tube as a function of force applied on the tube.

$$U(r_{ij}) = Ae^{-\lambda_1 r_{ij}} - Be^{-\lambda_2 r_{ij}}\left[1 - D\left\{\sum_k (h - \cos\theta_{ijk})^2\right\}^n\right] \tag{13}$$

where, D, a constant, has the value 0.49486792.

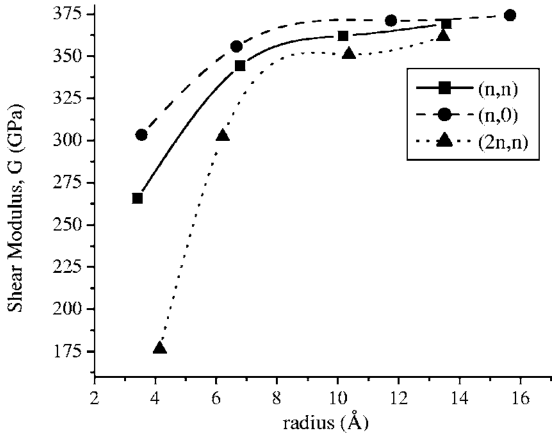

FIG. 5. Shear modulus for various tubes. (dots are calculated points, curves are a guide to the eye).

As a test case, then we take a graphene sheet and numerical accuracy of this form is tested for two cases; in first case taking only bond deformation, and in the second case considering only the bond bending.

Considering the bond angles to be fixed, we get PE as

$$U = U_o + x\left(\frac{\Delta l}{l_o}\right)^2,$$

and for rigid bonds, PE can be written as

$$U = U_o + y\delta^2.$$

We find a close agreement, as shown in Table V, between the values that were obtained numerically and those which were obtained using this approximate form, thereby confirming its numerical accuracy.

We then apply this modified form to find Young's modulus and Poisson ratio of a graphene sheet using the expression in Eq. (13), quite conveniently, shown in Appendix A. Young's modulus and Poisson ratio comes out to be 1.272 TPa and 0.147, respectively. While from numerical work described above, they are 1.29 TPa and 0.16, respectively. These are tabulated in Table V.

Similarly, algebraic estimates may be made of moduli of the various tubes, which would take the load off computational efforts.

V. EFFECT OF PRESSURE APPLIED LATERALLY ON A SINGLE-WALLED NANOTUBE

Upon applying the lateral pressure on a SWNT by shrinking and expanding the radius of the tube, the tube is again minimized to get the stable structure, and thus we find the PE as a function of lateral strain, shown in Fig. 6. We found that upon applying the pressures that we are working with, i.e., of GPa range, the axial deformation produced in the tubes is negligibly small and this has repercussions while studying the effect of pressure on bundles.

VI. EFFECT OF THE PRESSURE APPLIED ON THE ROPES

In a bundle consisting of identical nanotubes, they are arranged in a two-dimensional hexagonal close packed struc-

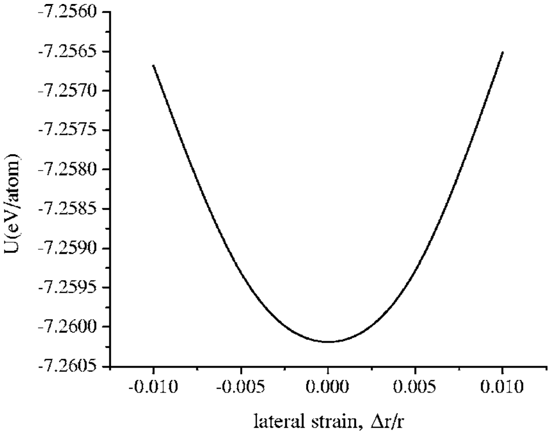

FIG. 6. PE as a function of lateral strain.

TABLE V. Comparison of the numerical values and those obtained using the approximate form of Brenner potential.

	x (eV)	y (eV)	Young's modulus (TPa)	Poisson ratio
Numerical calculations	59.63	14.733	1.29	0.16
Analytical calculations	60.38	15.3	1.272	0.147

ture (forming "nanoropes"), interacting via weak van der Waals (vdW)-type attractive forces, shown in Fig. 7(a). Usually, the cylindrical tubes are assumed to be circular in cross section. However several authors, on general considerations, predicted them to be deformed either elliptically or having facets due to the vdW forces between the neighboring tubes in a bundle, shown in Figs. 7(b) and 7(c).

These deformations are prominent for larger diameter tubes or when an external strain is applied perpendicular to the long axis of the tubes. Even an isolated tube assumes a flattened or collapsed structure whose extent depends largely on the diameter of the tube.[16] Further, it is harder to distort a MWNT than a SWNT.[17]

As the hydrostatic pressure is applied on a bunch, the axial deformation is very small as presented in Sec. V and therefore, we have considered only the bond bending and deformation of tubes. As the applied hydrostatic pressure on a bunch is increased, the tubes move closer together, moving against vdW forces. When two neighboring tubes are sufficiently close, they may flatten because of strong repulsive forces at short distances. This flattening increases the area of contact, whereby a larger number of atoms come closer, lowering the energy via vdW interaction. However, this also increases the curvature at the corners. Figure 7(c) shows the expected cross section of the tubes once such a flattening has taken place, taking into account the fact that each tube is surrounded by six neighbors, hence six-sided faceting. The increase in curvature results in the mechanical energy of bending being raised. These two processes compete in energy. In order to study this, we model the distorted (or faceted) tube with the help of a distortion factor f. A fraction f of the total area of a tube is in six flat portions and the rest is comprised of six rounded corners. The cross section of such tubes corresponding to different values of f are shown in Fig. 8(a). The excess energy of bending of such a distorted tube over one with circular cross section, using Eq. (2), is given by

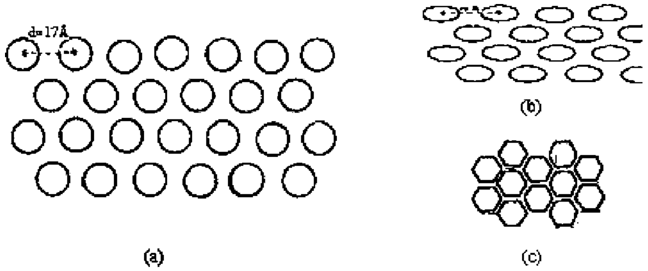

FIG. 7. Cross section through bundle of nanotubes: (a) Undistorted tube cross section, (b) elliptically deformed tubes, and (c) faceted tubes.

$$U_{\text{bending}} = \pi c_o L\left(\frac{1}{\rho} - \frac{1}{r}\right), \tag{14}$$

where r is the radius of the undistorted (circular cross section) tube and ρ is the radius of curvature at the corner after distortion (faceting). ρ depends on the deformation parameter as $\rho=(1-f)r$. L is the length of the tube under consideration. We show later that f plays the role of order parameter for a faceting phase transition. We first evaluate the lattice energy of such a bunch. We consider parallel identical tubes with a given f, arranged on a close-packed two-dimensional lattice [Fig. 7(a)]. Instead of using the atom-atom interactions for this calculation, we have used the continuum shell approximation in which each tube is supposed to be comprised of a large number, N, of evenly distributed thin parallel rods or lines of C atoms parallel to the axis [Fig. 8(b) and 8(d)]. The linear density of C atoms on each rod depends on the number of rods being used, since the areal density of the C atoms on a tube wall is a constant. To find the total interaction energy of this lattice, we sum over interactions between all rod-rod pairs in the system, except intratube interactions, i.e.,

$$U_{\text{tot}} = \frac{1}{2}\sum_{i,j}{}' V_{ij}, \tag{15}$$

where prime excludes ij pair belonging to same tube. The interaction V_{ij} is obtained by integrating the six-exponential potential over two parallel lines separated by a distance r

$$U(r) = -\frac{A}{r^6} + Be^{-\alpha r}, \tag{16}$$

where the interaction parameters A, B, and α are 358 kcal mol^{-1} Å^6, 42000 kcal mol^{-1}, and 3.58 Å^{-1}, respectively, as provided by Kitaigorodsky.[30] Integrating this expression over two parallel lines, we get

$$U_{ij} \equiv U(r_{ij}) = \left[-\frac{3\pi}{8}\frac{A}{r_{ij}^5} + 2Br_{ij}K_1(\alpha r_{ij})\right]\lambda^2 L, \tag{17}$$

where L is the length of each tube, infinitely long in the limit, λ is the linear density of the C atoms on each rod, K_1 is a modified Bessel function, and r_{ij} denotes the distance between the two parallel rods. From Fig. 8(c), the distance, r_{ij} is given by

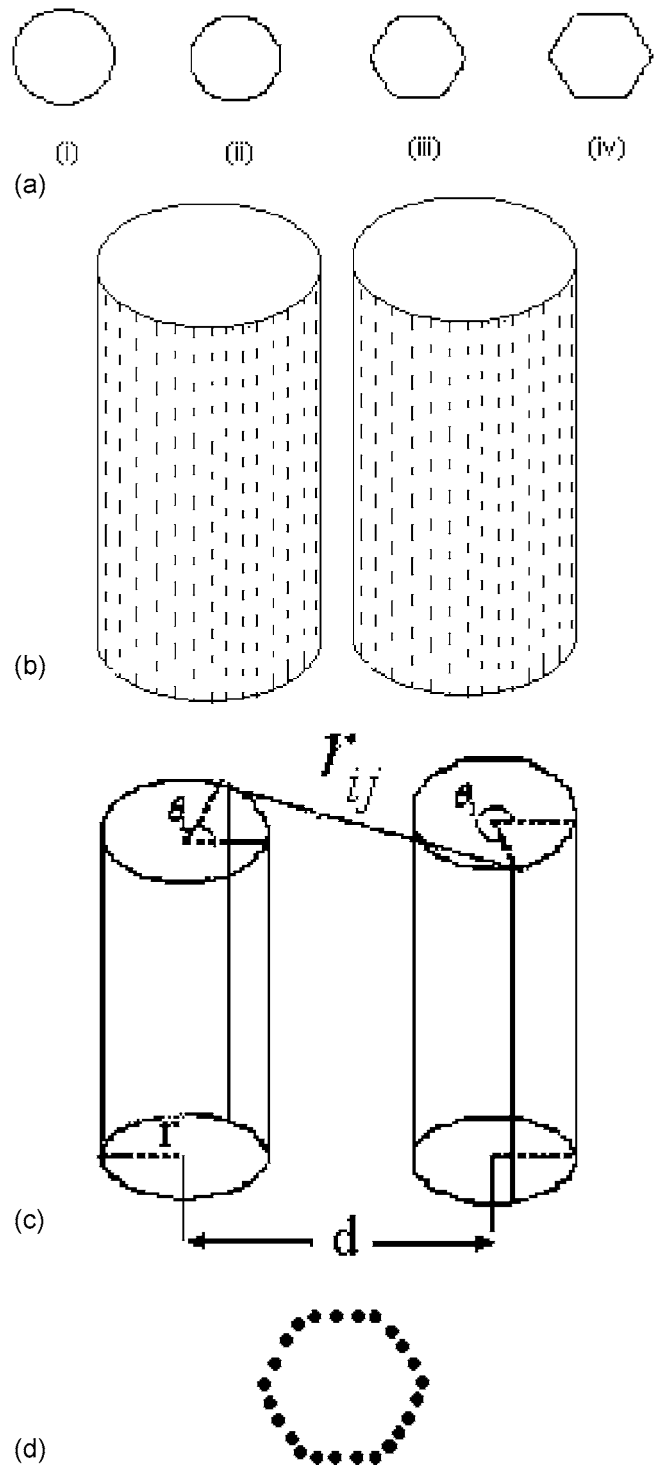

FIG. 8. (a) Cross sections for tubes of various distortion, with factor f=(i) 0.0, (ii) 0.3, (iii) 0.6, and (iv) 0.9. (b) Two identical nanotubes showing lines of C-atoms parallel to the axis. (c) Two rods on two tubes showing r_{ij}. (d) Cross section of a faceted tube. Each dot represents a rod of C atoms. The larger the number of dots, the closer the model to continuum limit.

$$r_{ij} = \sqrt{(d + r\cos\theta_2 - r\cos\theta_1)^2 + (r\sin\theta_2 - r\sin\theta_1)^2}.$$

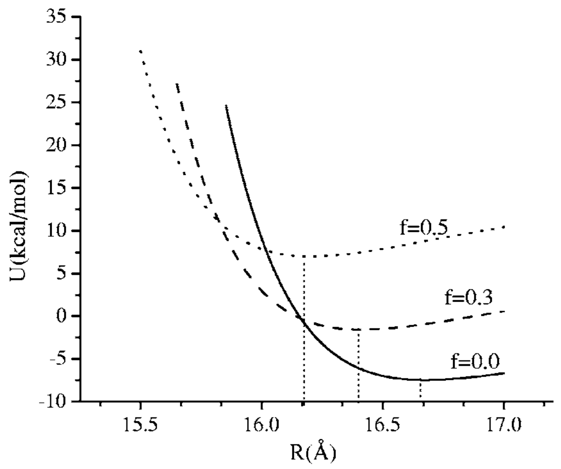

FIG. 9. The interaction energy between two bucky tubes. The three curves are for circular cross section, slightly distorted (faceted), and dominantly faceted tube cross sections.

Each rod is, however, not continuous and is made up of atoms. We take it to be continuous as the continuum model has successfully reproduced the bulk and lattice properties of C_{60} and C_{70} solids in the past.[31,32] We can calculate the interaction energy between two SWNTs by assuming a smeared out continuous tube model having a uniform distribution of carbon atoms on their surfaces and integrating C—C interactions over this distribution. However, instead of doing this integration, we have performed the numerical summation over interactions of rods of a given tube with the rods of its neighbors to get the total tube-tube interaction.

The lattice energy of such a configuration is found by numerically summing over interactions of rods of a given tube with those of all its neighbors. We performed the calculations taking varying number of rods per tube and find that 48 rods per tube and a lattice distance of one neighbor gives sufficient numerical accuracy for studying energies and phase transitions. Here, the calculations are given for 13.56 Å diameter tubes, corresponding to (10,10) CNTs.

To the lattice energy thus obtained, we add the bending energy of the distorted tubes according to Eq. (10). We thus obtain $U(f,d)$, the total energy of the lattice as a function of lattice size, given by d, and the distortion parameter f. For a given f, the equilibrium lattice constant d_o is obtained by plotting U against d and identifying coordinates where the minimum of energy occurs. Figure 9 shows such minima for three values of $f-d_o(0)$, $d_o(0.3)$, and $d_o(0.5)$. These same curves are used to find pressure, as follows. At zero pressure, the system would be in equilibrium with $d=d_o$. However, when compressed, it would acquire a state with d such that

$$U = U_o + P\Delta V, \tag{18}$$

such that

$$\Delta V = \sqrt{3}(d_o^2 - d^2), \tag{19}$$

where we have used $V=\sqrt{3}d^2$, V being volume per tube per unit length.

Thus, from the given curve (Fig. 9) for U versus d, we get U versus P. This U [Eq. (18)] is the Helmholtz free energy at $T=0$ by definition. At a given P, when one compares free energy $U(f)$ for all f, the stable system is given by minimum

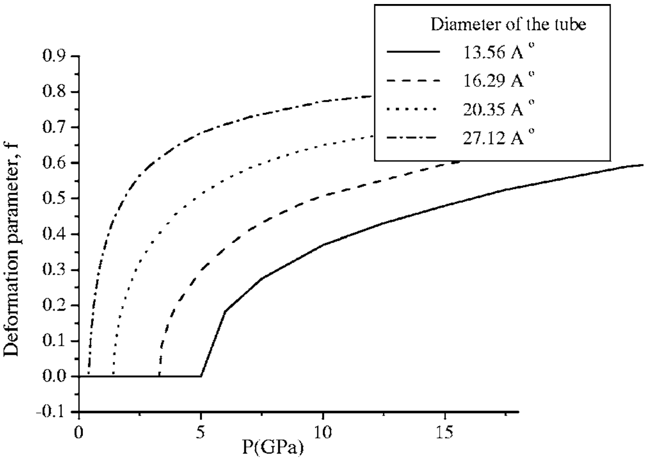

FIG. 10. Deformation parameters corresponding to stable configurations at various pressures.

$U(f)$, i.e., system adopts that f for which U is minimum for that pressure. This yields f versus P curve, Fig. 10. This shows that for $P<P_c$, $f=0$, gives a stable configuration; whereas for $P>P_c$, f rises as P increases. At $t=0$, P_c is the initial point where the order parameter f begins to rise above zero. Once we have f versus P for a particular P, we can pick up R corresponding to appropriate f. Thus, we have d^2 (or V) versus P. This is shown in Fig. 10. The P-V curve has a kink at P_c.

However, we have repeated this calculation for various tube diameters and found out the critical pressure corresponding to each tube. From our model, we found that about 34 Å diameter tubes show faceting even at ambient conditions, however Tersoff,[33] using the valence force model for atomic interactions within the tube and 6-12 potential for vdW interactions, found this for 25 Å diameter tubes and Lopez *et al.*,[21] from MD simulations with short-range Tersoff's potential and long-range many-body potential, conclude that polygonization can be observed, under proper conditions, in tubes as small as 17 Å, and remarked it should be observed more frequently in bundles of tubes of larger diameters.

Phase transition also depends on the value of the elastic bending constant. A lower value of this constant makes the discontinuity in the compressibility curve come at a lower pressure, e.g., $c_o=15$ kcal/mole corresponds to a transition at a pressure$=1.7$ GPa. However, for Brenner potential used by us, $c_o=35.5$ kcal/mole.

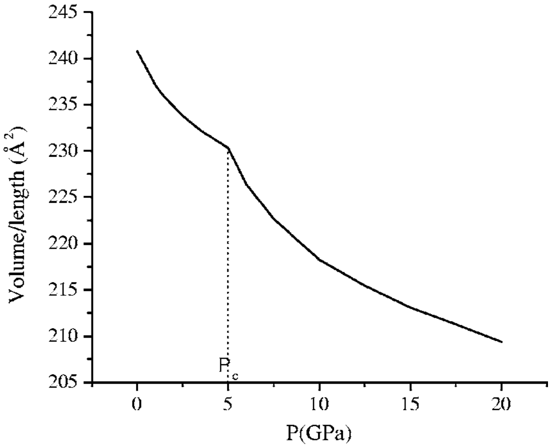

FIG. 11. Variation of volume with pressure.

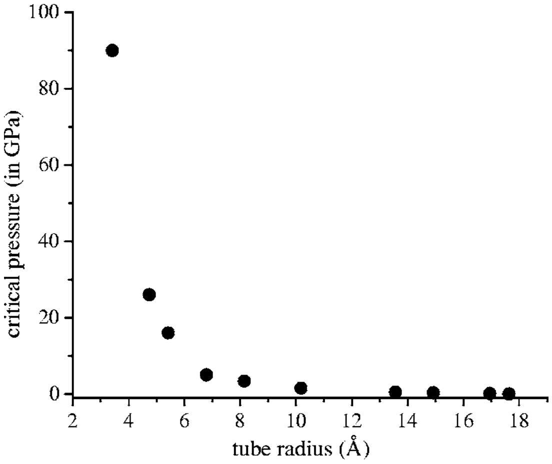

FIG. 12. Critical pressure (P_c) for phase transition between circular and faceted tube cross sections in a bunch, shown for various tube diameters.

Similarly, the compressibility, K, is obtained from the P-V curve as

$$K=-\frac{1}{V}\frac{\partial V}{\partial P}. \tag{20}$$

This quantity also shows a huge discontinuity at P_c (see Figs. 11–13).

VII. YOUNG'S MODULUS OF SINGLE-WALLED NANOTUBE ROPES-UNDEFORMED AND DEFORMED

When pressure is applied laterally to a rope, the tubes become faceted at and above a critical pressure P_c. If we denote by Y_t, the Young's modulus of a single SWNT in the bunch, then that of the rope, Y_r, is a simple function of Y_t and the lattice distance d between two nearest-neighbor tubes. This is given by Eq. (24) which is derived as follows.

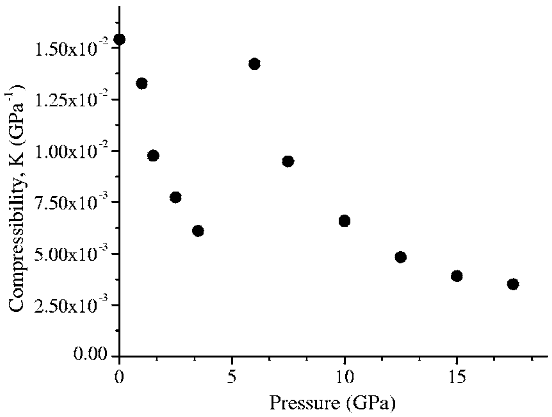

FIG. 13. Variation of compressibility with pressure. The solid points represent the points at which calculation was made.

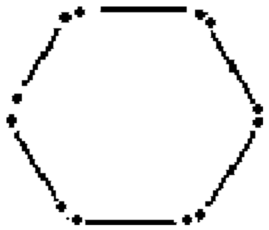

FIG. 14. A faceted SWNT where the solid lines represent the graphene sheet and dotted lines represent the parts of a tube.

If F/A denotes the force (directed along the tubes' axes) per unit area of a SWNT rope, then the force per rope is given by

$$\varphi = \frac{F}{A}\frac{\sqrt{3}}{2}d^2. \tag{21}$$

The second factor on the rhs is the area per tube in the cross section of the rope [Fig. 7(a)], where d denotes the nearest-neighbor distance in this lattice. If the rope (as well as all its constitutent SWNTs) suffers elongation Δl, its original length being l_o, then

$$Y_r = \frac{F/A}{\Delta l/l_o}. \tag{22}$$

We have defined Young's modulus of a tube, Y_t, as

$$Y_t = \frac{\varphi/a_o}{\Delta l/l_o}, \tag{23}$$

where $a_o = 2\pi r t$, as in Eq. (6). Thus, Y_r and Y_t are related as

$$Y_r = \frac{2a_o}{\sqrt{3}d^2}Y_t. \tag{24}$$

For single tubes which have undeformed circular cross sections, a SWNT has been studied in Sec. III for no lateral pressure and in Sec. V incorporating lateral pressure. For a bunch, when lateral pressure $P < P_c$, the intertube spacing d decreases and according to Eq. (24), Y_r changes. For $P > P_c$, in addition to d, shape of the SWNTs also change, causing a change in Y_t. Y_t for a deformed tube is calculated, making use of Y_o, that of a graphene sheet and a knowledge of $Y(r)$, Young's modulus of tubes of varying circular cross sections of radius r. This estimate is presented below.

Since a deformed tube is comprised of six sheets of graphene (shown as a solid line in Fig. 14) and six pieces of 1/6th fraction of tube (shown as dotted lines in Fig. 14), change in energy of the deformed tube after stretching by an amount Δl is given by

$$\Delta U = \Delta U_g + \Delta U_t, \tag{25}$$

where ΔU_g denotes the change in energy of the graphene sheet and ΔU_t is the change in energy of a tube of radius r', which is the radius of the effective tube after deformation. We have $r' = r(1-f)$, where f is the deformation parameter or distortion factor.

Using the standard expression for any wire,

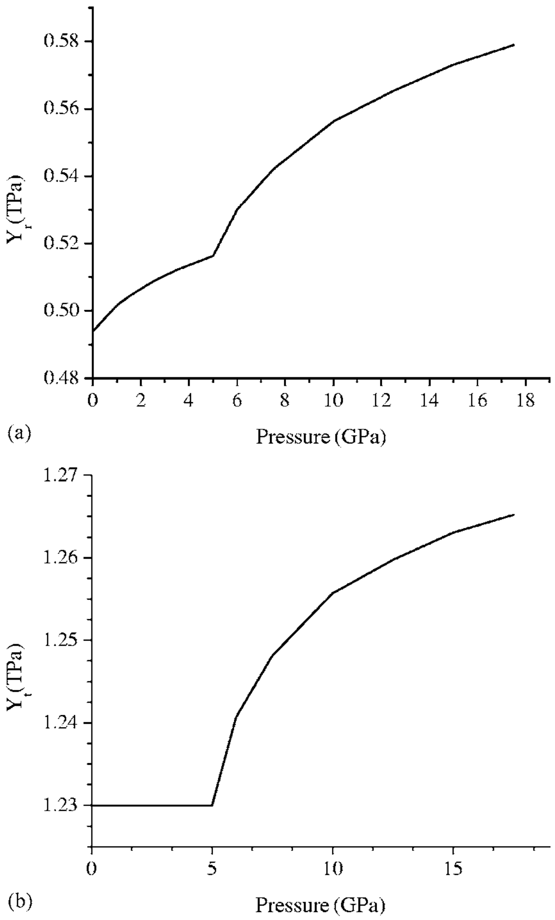

FIG. 15. (a) Pressure dependence of Young's modulus of a nanorope of (10,10) tubes. (b) Pressure dependence of Young's modulus for a single (10,10) tube.

$$\Delta U = \frac{1}{2}Y\frac{a}{l}(\Delta l)^2. \tag{26}$$

We express the energy of the whole deformed tube as

$$\Delta U = \frac{1}{2}Y_o\frac{f(2\pi r)t}{l}(\Delta l)^2 + \frac{1}{2}Y(r')\frac{(1-f)(2\pi r)t}{l}(\Delta l)^2, \tag{27}$$

where r is the radius of the undeformed tube and t is the usual sheet/wall thickness taken to be 3.4 Å in this work. From this expression, Young's modulus of the deformed SWNT is given as

$$Y_t = Y_o f + Y(r') \,.\, (1-f), \tag{28}$$

where, Y_o is the Young's modulus of graphene sheet, which by our calculations comes out to be equal to 1.29 TPa, and $Y(r')$ is Young's modulus of a tube of radius r'. The value of f changes with pressure, and hence Y_t. At pressures $P < P_c$, $f = 0$

$$Y_t = Y(r') = Y(r).$$

The variation of Y_t with pressure for a (10,10) tube is shown in Fig. 15(b).

TABLE VI. Calculated and measured values of Young's modulus.

Reference	Young's modulus (TPa) and wall thickness
Treacy *et al.* (Ref. 2)	1.8
Krishnan *et al.* (Ref. 3)	1.3
Wong *et al.* (Ref. 4)	1.28
Hernandez *et al.* (Ref. 7)	1.24 (3.4)[a]
Minami *et al.* (Ref. 8)	1.06
Zhou *et al.* (Ref. 9)	5.1 (0.71)[a]
Sears and Batra (Ref. 10)	2.3–2.6 (1.34)[a]
Lu (Ref. 14)	0.97 (3.4)[a]
Yakobson *et al.* (Ref. 26)	5.5 (0.66)[a]
This work.	1.24 (3.4)[a]

[a] The quantity in parantheses gives the value of wall thickness in Å taken by respective calculations.

The young's modulus of a nanorope, consisting of (10,10) tubes, as a function of pressure is shown in Fig. 15(a).

VIII. DISCUSSION AND CONCLUSIONS

Young's modulus, shear modulus, and Poisson ratios of a variety of tubes having different chiralities and sizes have been obtained using the Tersoff–Brenner potential for the interaction between C atoms. Since these elastic moduli depends on the wall thickness of the tubes as we are considering it to be a hollow cylinder, we take it to be equal to 3.4 Å, equal to the adjacent layer separation in graphite. Yakobson *et al.*[26] and Zhou *et al.*,[9] however, assume the pi-bond length 0.66 Å as a better choice for wall thickness. However, for Young's modulus of nanoropes, such considerations are not required, as we can use area of the cross section of the whole rope. In the case of SWNTs, how to choose this value remains a question for experimentalists as well as theoreticians as it is necessary to interpret the experimental observations on the basis of some mechanical model, usually a hollow cylinder with a certain wall thickness. The values thus obtained for Young's modulus and shear modulus come out to be in close agreement with other authors works. The value of Y is in very good agreement with the experimental value obtained by Krishnan and co-workers[3] for SWNTs (1.25 TPa). It is also in rather good agreement with the value reported by Wong *et al.*[4] of 1.28 TPa for MWNTs. But since Young's modulus depends mainly on intratube interactions, values for MWNT and SWNT should be expected to be quite similar. However, the values given by Lu *et al.*[14] are somewhat smaller than others (~.97 TPa). The Young's modulus given by these authors and that obtained by us are tabulated in Table VI for comparison. All calculated values of Young's modulus when scaled by the factor equal to the area of cross section of their respective calculations converge to similar values. The shear modulus also comes out to be in close agreement with those given by Yu from MD simulations. Our results agree with the expectation that the value of moduli are smaller for small diameter tubes and in the limit of large radii, these values correspond to that of graphene sheet. Next, we show that the strain dependence of Y, $\partial Y/\partial\varepsilon$, is equal to -7.5 TPa at $\varepsilon=0$ and equals -3.6 TPa at $\varepsilon=0.05$.

According to Newton's formula, the velocity of sound is related to Young's modulus and density of the material ρ as, $v=\sqrt{Y/\rho}$ and the value of Y for (10,10) tube corresponds to velocity of longitudinal sound$=1.995$ cm/μs.

After studying the axial effects in a SWNT under pressure, we have applied the pressure changes in a nanorope. The discontinuity in the compressibility curve indicates a structural phase transition at a pressure of about 5 GPa. Since the order parameter f changes continuously across P_c, though its first derivative is discontinuous, we identify it as a second-order phase transition.

This result is not very compatible with the values obtained experimentally, but the work presented here gives a good qualitative understanding of the pressure induced phase transitions. From our model, we found that about 34 Å diameter tubes show faceting even at ambient conditions; however, Tersoff[33] found this for 25 Å diameter tubes and Lopez *et al.*[21] observed this faceting for 17 Å tubes. This indicates that the continuum model, used by us for making calculations, make the tubes a little harder, thereby explaining the transition appearing at a higher pressure than observed experimentally. We next calculate the Young's modulus of the rope, making use of Y found earlier for the SWNTs. This value ($\cong 0.495$ TPa) is in close agreement with the value of 0.563 TPa given by Lu[13] for nanoropes consisting of (10,10) tubes. The curve, Fig. 13, showing the pressure dependence of Y_r, shows a discontinuity at the phase transition.

Finally, the Brenner potential modified and is reduced to a much convenient form, using certain approximations, with sacrifice in the numerical accuracy only upto 4%. Using this form, it is possible to calculate the Young's modulus and Poisson ratio of graphene sheet analytically and is compared well with the values obtained numerically using the original form of Brenner potential. This form can thus make the computations much easier and handy. With this form, bond bending and bond stretching can be easily understood quantitatively since we can compare both of them through their coefficients which is not possible to do numerically.

In full quantum mechanical calculations, some variations may be present, albeit it is likely that these deviations are small, especially for larger radius tubes. These deviations also affect the geometry of the tubes, which also deviate from the ideal.[34] However, these deviations are not significant while studying the lattice dynamical properties and have a role to play in electronic structure calculations.

In conclusion, we have investigated elastic properties of nanotubes and nanoropes using an empirical pair potential. A SWNT is much stiffer than steel for which the Young's modulus is about 200 GPa. We use the hydrostatic pressure as a probe to study the radial deformations of the nanotubes. We find that these crystalline nanoropes are highly anisotropic as far as their elastic properties are concerned. These are very soft radially and stiff in the axial direction and these properties of nanoropes—light, flexible, and stiff make them promising candidates for composite materials. The strain dependence of Young's modulus of SWNTs and pressure dependence of Young's modulus of nanoropes have been studied for the first time. These show interesting features at some critical pressure values which motivates further experimental work on pressure dependent studies of Young's modulus, both for SWNTs and nanoropes.

ACKNOWLEDGMENTS

One of the authors (S.G.) acknowledges the financial support from CSIR, New Delhi.

APPENDIX A

From Eq. (1), within bond limits, $f_c(r_{ij})$ can be taken equal to one for r_{ij} pair and so the Brenner potential is given as:

$$U(r_{ij}) = Ae^{-\lambda_1 r_{ij}} - b_{ij}Be^{-\lambda_2 r_{ij}}, \tag{A1}$$

where b_{ij} has the following form:

$$b_{ij} = \frac{1}{(1+\beta^n \varsigma_{ij}^{n})^{1/2n}}, \tag{A2}$$

where

$$\zeta_{ij} = \sum_k g(\theta_{jk}), \tag{A3}$$

with $g(\theta)=1+c^2/d^2-c^2/d^2+(h-\cos\theta)^2$.

In Eq. (A3) the summation over k runs over neighbors of i leaving out j, and θ_{ijk} is the angle between bonds ij and ik. For a hexagonal sheet, not too badly deformed, θ remains close to $2\pi/3$. Therefore, $(h-\cos\theta)\approx -.07$, and, d being equal to 4.3484,

$$\left\{\frac{(h-\cos\theta)}{d}\right\}^2 < 1.$$

Making use of c, d, and g quoted in Table I, we have

$$g(\theta) \cong 1 + \frac{c^2}{d^2}\left\{\frac{h-\cos\theta}{d}\right\}^2 \cong O(10^4) \tag{A4}$$

and

$$\beta\sum_k g(\theta_{ijk}) \cong O(10^{-3}). \tag{A5}$$

Substituting this into Eq. (A2), we get

$$b_{ij} = [1+(\beta\zeta_{ij})^n]^{-1/2n} \cong 1 - \frac{\beta^n}{2n}\left[\sum_k\left\{\frac{c(h-\cos\theta_{ijk})}{d^2}\right\}^2\right]^n \tag{A6}$$

Equation (A1) can now be written as

$$U(r_{ij}) = Ae^{-\lambda_1 r_{ij}} - Be^{-\lambda_2 r_{ij}}\left[1 - D\left\{\sum_k (h-\cos\theta_{ijk})^2\right\}^n\right] \tag{A7}$$

where $D=1/2n(\beta c^2/d^4)^n=0.49486792$.

Now, for a hexagonal network, k runs over two neighbors, i.e., $k=1,2$. For both of these, in an undistorted network, $\theta = 120°$. From Eq. (A7), $U(r_{ij})=Ae^{-\lambda_1 r_{ij}}-0.9827Be^{-\lambda_2 r_{ij}}$. This holds for all the bonds in the plane. The equilibrium bond length is given by

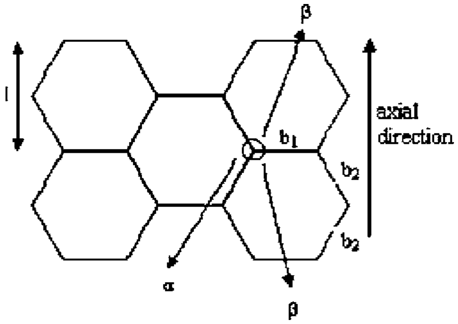

FIG. 16. A section of graphene sheet showing various bonds and bond angles.

$$b_o = \frac{1}{\lambda_1-\lambda_2}\ln\left(\frac{\lambda_1 A}{0.9827\times\lambda_2 B}\right) = 1.422A^{\circ}.$$

If we use the original Eq. (A1), one gets $b_o=1.4217A°$, which corroborates the approximations that we used to reach this much simplified expression.

Now consider a graphene sheet having bond length equal to b_o and $\theta=120°$ (see Fig. 16). Upon applying the force in the axial direction, the bond lengths become b_1 and b_2 where

$$b_1 = b_o + \Delta_1, \quad b_2 = b_o + \Delta_2;$$

and the bond angles become

$$\alpha = 120^{\circ} + \delta, \quad \beta = 120^{\circ} - \delta/2.$$

The length of the hexagon is given by

$$l = 2b_2\sin\frac{\theta_2}{2} = 2b_2\sin\left(\frac{120^{\circ}+\delta}{2}\right) \cong 2(b_o+\Delta_2)\left[\frac{\sqrt{3}}{2}+\frac{\delta}{4}\right]. \tag{A8}$$

In the undistorted sheet, the length is

$$l_o = \sqrt{3}b_o. \tag{A9}$$

Thus, we have the change in length per hexagon as

$$\Delta l \cong \sqrt{3}\Delta_2 + \frac{b_o}{2}\delta \text{ (up to first-order in small quantities)}. \tag{A10}$$

The above two equations yield

$$\frac{\Delta l}{l_o} = \frac{\Delta_2}{b_o} + \frac{\delta}{2\sqrt{3}}, \quad \text{or,} \tag{A11}$$

$$\Delta_2 = \frac{\Delta l}{\sqrt{3}} - \frac{b_o}{2\sqrt{3}}\delta. \tag{A12}$$

The width of the hexagon is given by

$$W=2b_1+2b_2\cos\left(60^\circ+\frac{\delta}{2}\right)\cong 3b_o+2\Delta_1+\Delta_2-\frac{\sqrt{3}}{2}b_o\delta, \tag{A13}$$

whereas in undistorted sheet,

$$W_o=3b_o. \tag{A14}$$

So, we have

$$\frac{\Delta W}{W_o}=\frac{2\Delta_1+\Delta_2}{3b_o}-\frac{\delta}{2\sqrt{3}}. \tag{A15}$$

Each atom is attached to two b_2 and one b_1 type bonds. Therefore, energy per atom in the stretched sheet,

$$U=\frac{(2U(b_2)+U(b_1))}{2}=U(b_2)+\frac{1}{2}U(b_1). \tag{A16}$$

Now,

$$\begin{aligned}U(b_1)&=Ae^{-\lambda_1 b_1}-\lfloor 1-D\{2(h-\cos\beta)^2\}^n\rfloor Be^{-\lambda_2 b_1}\\&=Ae^{-\lambda_1 b_1}-[1-2^nD\{(h-\cos 120^\circ)\\&\quad+(\cos 120^\circ-\cos\beta)\}^{2n}]Be^{-\lambda_2 b_1}\\&=Ae^{-\lambda_1 b_1}-\Bigg[1-2^nD(h-\cos 120^\circ)^{2n}\\&\quad\times\left\{1+2n\frac{\cos 120^\circ-\cos\beta}{h-\cos 120^\circ}\right\}\Bigg]Be^{-\lambda_2 b_1}\end{aligned}$$

$$(\text{provided } |\cos 120^\circ-\cos\beta|\ll|h-\cos 120^\circ|), \tag{A17}$$

and,

$$\begin{aligned}U(b_2)&=Ae^{-\lambda_1 b_2}-\lfloor 1-D\{(h-\cos\alpha)^2\\&\quad+(h-\cos\beta)^2\}^n\rfloor Be^{-\lambda_2 b_2}\\&=Ae^{-\lambda_1 b_2}-\Bigg[1-D\Bigg\{(h-\cos 120^\circ)^2\\&\quad\times\left(1+\frac{\cos 120^\circ-\cos\alpha}{h-\cos 120^\circ}\right)^2\\&\quad+(h-\cos 120^\circ)^2\\&\quad\times\left(1+\frac{\cos 120^\circ-\cos\beta}{h-\cos 120^\circ}\right)^2\Bigg\}^n\Bigg]\\&\quad Be^{-\lambda_2 b_2}.\end{aligned} \tag{A18}$$

Now, $\cos 120^\circ-\cos\alpha=\cos 120^\circ-\cos(120^\circ+\delta)\cong-\delta^2/4+\sqrt{3}/2\delta$ and $\cos 120^\circ-\cos\beta\cong-\delta^2/16-\sqrt{3}/4\delta$.

Define the quantities G, H, $\bar{G}$, $\bar{B}$, and J as,

$$G\equiv 2^nD(h-\cos 120^\circ)^{2n},\quad H\equiv\frac{2n}{h-\cos 120^\circ},$$

$$\bar{G}\equiv\frac{GH}{4(1-G)},\quad \bar{B}\equiv B(1-G),\quad J\equiv\frac{\bar{G}(15+3(n-1))}{16(h-\cos 120^\circ)}, \tag{A19}$$

and put $b_1=b_o+\Delta_1$, $b_2=b_o+\Delta_2$.

We then obtain,

$$\begin{aligned}U(b_1)&\cong Ae^{-\lambda_1 b_o}\left(1-\lambda_1\Delta_1+\frac{1}{2}\lambda_1^2\Delta_1^2\right)-\Bigg[1+\bar{G}\Bigg(\sqrt{3}\delta\\&\quad-\frac{\delta^2}{4}\Bigg)\Bigg]\bar{B}e^{-\lambda_2 b_o}\left(1-\lambda_2\Delta_1+\frac{1}{2}\lambda_2^2\Delta_1^2\right),\end{aligned} \tag{A20}$$

$$\begin{aligned}U(b_2)&\cong Ae^{-\lambda_1 b_o}\left(1-\lambda_1\Delta_2+\frac{1}{2}\lambda_1^2\Delta_2^2\right)-\Bigg[1+\bar{G}\left(-\frac{\sqrt{3}}{2}\delta\right)\\&\quad-J\delta^2\Bigg]\bar{B}e^{-\lambda_2 b_o}\left(1-\lambda_2\Delta_2+\frac{1}{2}\lambda_2^2\Delta_2^2\right).\end{aligned} \tag{A21}$$

From Eqs. (A16), (A20), and (A21), we get

$$\begin{aligned}U&=U_o+\Delta_1^2\left\{\frac{A}{4}\lambda_1^2e^{-\lambda_1 b_o}-\frac{\bar{B}}{4}\lambda_2^2e^{-\lambda_2 b_o}\right\}+\Delta_2^2\Bigg\{\frac{A}{2}\lambda_1^2e^{-\lambda_1 b_o}\\&\quad-\frac{\bar{B}}{2}\lambda_2^2e^{-\lambda_2 b_o}\Bigg\}+\delta^2\bar{B}e^{-\lambda_2 b_o}\left(J+\frac{\bar{G}}{8}\right)\\&\quad+\delta\Delta_1\left(\frac{\sqrt{3}}{2}\lambda_2\bar{G}\right)\bar{B}e^{-\lambda_2 b_o}-\delta\Delta_2\left(\frac{\sqrt{3}}{2}\lambda_2\bar{G}\right)\bar{B}e^{-\lambda_2 b_o}\end{aligned} \tag{A22}$$

where $U_o=\frac{3}{2}(Ae^{-\lambda_1 b_o}-\bar{B}e^{-\lambda_2 b_o})$ is the energy per atom of an unstretched sheet.

On evaluating various coefficients, we get

$$\begin{aligned}U&=U_o+9.9826\Delta_1^2+19.96517\Delta_2^2+15.3\delta^2-2.4232\Delta_1\delta\\&\quad+2.4232\Delta_2\delta\end{aligned} \tag{A23}$$

Using Eq. (A23), we first consider the case of rigid bond angles, i.e., $\delta=0$. We further put $\Delta_1=\Delta_2$ and get

$$U=U_o+29.94777\Delta^2=U_o+29.94777b_o^2\left(\frac{\Delta}{b_o}\right)^2.$$

From Eq. (A11), for this case,

$$\frac{\Delta l}{l_o}=\frac{\Delta}{b_o}.$$

$$\text{Therefore, } U=U_o+60.38\left(\frac{\Delta l}{l_o}\right)^2. \tag{A24}$$

However, from numerical calculations, with exactly same constraints, we obtain the curve shown in Fig. 17, which, fitted to a parabolic form, gives

$$U=U_o+.00371\left(\frac{\Delta l}{l_o}\right)^2l_o^2=U_o+59.63\left(\frac{\Delta l}{l_o}\right)^2. \tag{A25}$$

Similarly, by putting $\Delta_1=\Delta_2=0$ in Eq. (A23) (the case of rigid bonds), we get

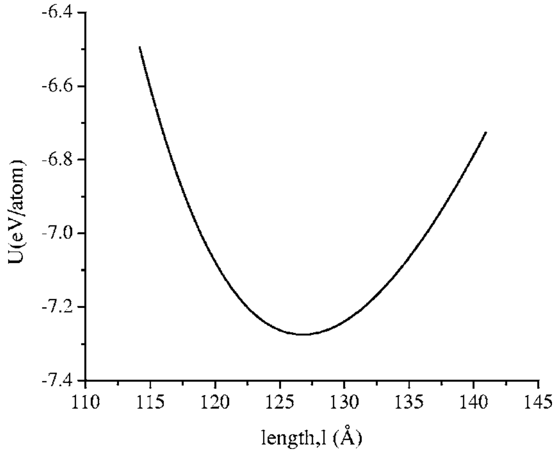

FIG. 17. Variation of energy with length of the graphene sheet obtained by changing the bond length (keeping $\Delta_1 = \Delta_2$).

$$U = U_o + 15.3\delta^2 \tag{A26}$$

From numerical calculations, we obtain the curve shown in Fig. 18. This curve can be fitted to

$$U = U_o + .011\left(\frac{\Delta l}{l_o}\right)^2 l_o^2.$$

Now, since $\Delta l/l_o = \delta/2\sqrt{3}$ [for $\Delta_1 = \Delta_2 = 0$, from Eq. (A11)]

$$U = U_o + 14.733\delta^2. \tag{A27}$$

The agreement between the numerically calculated and algebraically calculated coefficients verified our calculations.

Equation (A23) can further be written differently to represent the motion of a coupled harmonic oscillator and is given by

$$U = U_o + \frac{1}{2}C_1\Delta_1^2 + \frac{1}{2}C_2\Delta_2^2 + \frac{1}{2}P\delta^2 + K_1\Delta_1\delta + K_2\Delta_2\delta, \tag{A28}$$

where $C_1 = 19.965167$ eV/atom/Å^2, $C_2 = 39.9303342$ eV/atom/Å^2, $P = 30.6$ eV/atom, $K_1 = -2.4232$ eV/atom/Å, and $K_2 = 2.4232$ eV/atom/Å.

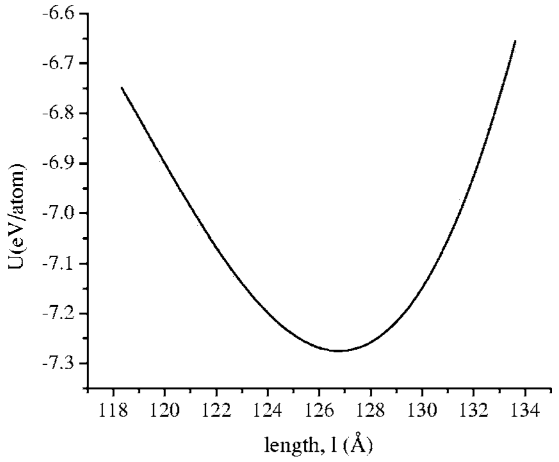

FIG. 18. Variation of energy with length of the graphene sheet obtained by distorting the bond angle.

Rewriting Eq. (A28),

$$\Delta U = \frac{1}{2}C_1\left(\Delta_1 + \frac{K_1}{C_1}\delta\right)^2 + \frac{1}{2}C_2\left(\Delta_2 + \frac{K_2}{C_2}\delta\right)^2 + \frac{1}{2}\bar{P}\delta^2, \tag{A29}$$

where $\bar{P} = P - K_1^2/C_1 - K_2^2/C_2$.

On putting the value of Δ_2 from Eq. (A12) in Eq. (A29), we get

$$\Delta U = \frac{1}{2}C_1\left(\Delta_1 + \frac{K_1}{C_1}\delta\right)^2 + \frac{1}{2}C_2\left(\frac{\Delta l}{\sqrt{3}} + \left(\frac{K_2}{C_2} - \frac{b_o}{2\sqrt{3}}\right)\delta\right)^2 + \frac{1}{2}\bar{P}\delta^2. \tag{A30}$$

On minimizing it with respect to Δ_1 and δ, we get

$$\Delta_1 = -\frac{K_1}{C_1}\delta, \quad \text{and} \tag{A31}$$

$$\delta = -\frac{\Delta l}{P'\sqrt{3}}\left(\frac{K_2}{C_2} - \frac{b_o}{2\sqrt{3}}\right). \tag{A32}$$

where $P' = (K_2/C_2 - b_o/2\sqrt{3})^2 + \bar{P}/C_2$.

From Eqs. (A30)–(A32),

$$\Delta U = Q\Delta l^2, \tag{A33}$$

where

$$Q = \frac{C_2}{6}\left[1 + \frac{1}{P'^2}\left(\frac{K_2}{C_2} - \frac{b_o}{2\sqrt{3}}\right)^2\left\{\left(\frac{K_2}{C_2} - \frac{b_o}{2\sqrt{3}}\right)^2 + \frac{\bar{P}}{C_2} - 2P'\right\}\right] = 5.7272 \text{ eV/atom/Å}^2. \tag{A34}$$

Equation (A33) can also be written as

$$\Delta U = 34.74 \times \left(\frac{\Delta l}{l_o}\right)^2. \tag{A35}$$

Now from numerical calculations, after fitting the curve (as shown in Fig. 19) showing the minimized energy corresponding to different lengths, we have

$$\Delta U = .0134 \times \left(\frac{\Delta l}{l_o}\right)^2 \times l_o^2 = 34.05\left(\frac{\Delta l}{l_o}\right)^2. \tag{A36}$$

This shows a quite good agreement of the values obtained numerically and those that we got algebraically.

Now, from Eqs. (A11), (A15), (A31), and (A32), the Poisson ratio is given by

$$\sigma = \frac{\dfrac{\Delta W}{W_o}}{\dfrac{\Delta l}{l_o}} = \frac{1}{3} + \frac{2}{3P'}\left[\frac{K_1}{C_1} + \frac{b_o}{\sqrt{3}}\right]\left(\frac{K_2}{C_2} - \frac{b_o}{2\sqrt{3}}\right). \tag{A37}$$

After putting the values of various constants, we get $\sigma = 0.147$ and, from Eq. (A29) the Young's modulus is obtained as

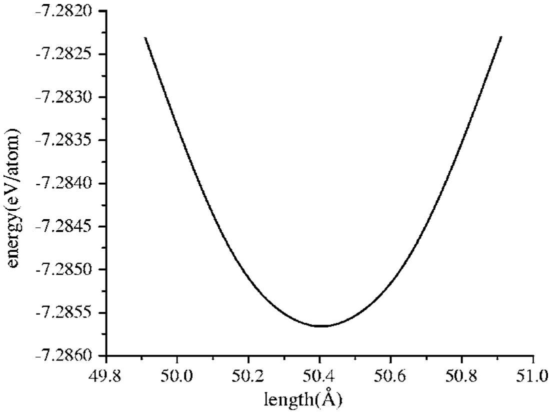

FIG. 19. Potential energy as a function of length of a graphene sheet.

$$Y=\frac{l}{a}\frac{\partial^2 U}{\partial l^2}=1.272\text{ TPa}. \tag{A38}$$

APPENDIX B

We will review the derivation and interpretation of the theory of torsion. We start by looking at a small section of length dx of a cylindrical tube under torsion, as shown in Fig. 20. During twisting, one end of the tube will rotate about the longitudinal axis with respect to the other end. The magnitude of this rotation is measured in terms of the angle in radians by which one end rotates relative to the other. This is called the "angle of twist." It can be seen that the line ab, which was initially horizontal, rotates through an angle γ, and moves to the line ab′. Here, $d\varphi$ is the angle of twist.

The shear strain, γ is the angle between ab and ab′ and is given by

$$\gamma=\frac{bb'}{ab}.$$

Using geometry, the arc length $\gamma dx=\rho d\varphi$, ρ is the radial distance to any point. Thus, we can write the strain as

$$\gamma=\rho\frac{d\varphi}{dx}. \tag{B1}$$

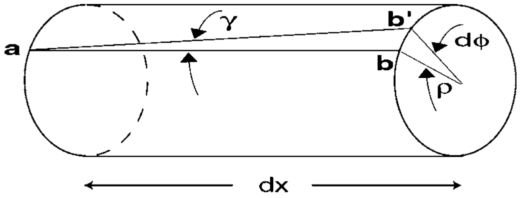

FIG. 20. A small section of a cylindrical tube.

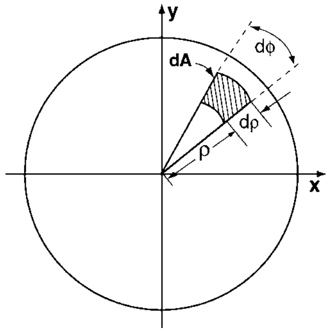

FIG. 21. A small cross section of the tube, showing a small area element.

For a tube of uniform cross section, thus the total twist, φ over a length L is simply

$$\varphi=L\frac{d\varphi}{dx}. \tag{B2}$$

Combining Eqs. (B1) and (B2), we get the final equation, giving the relation of shear strain to twist (φ), radial distance (ρ), and tube length (L). Note that all the relations here, are based solely on the geometry of the tube.

For a linear elastic material, using Hooke's law, we can write the shear stress as

$$\tau=G\gamma, \tag{B3}$$

where G is the shear modulus. The shear strain on a small area of material situated at a distance

$$\rho\text{ from the center, was found to be: }\gamma=\frac{\rho\varphi}{L}. \tag{B4}$$

$$\text{Thus, using Hooke's law, }\tau=\frac{G\rho\varphi}{L}. \tag{B5}$$

The torque, T, is calculated by integrating over the cross section the product of shear stress, τ, and the distance, ρ, from the center of the cylinder.

Substituting the stress from previous expressions, we find that torque is the integral of $\int_C G\varphi/L\rho^2 dA$ over the cross section of the tube. Pulling out the terms that do not vary over the cross section, we get

$$T=G\frac{\varphi}{L}J, \tag{B6}$$

where J is the polar moment of inertia and is defined as $J=\int_C\rho^2 dA$. Rearranging the terms, we can write the shear modulus as

$$G=\frac{TL}{\varphi J}. \tag{B7}$$

The moment of inertia about an axis perpendicular to the plane of an area is called the polar moment of Inertia. If dA is the area of a small element at a distance ρ from the center of the cross section, as shown in Fig. 21. then the polar moment of inertia, J, is defined as the integral over the cross section of the product of distance squared and the small area dA. For a hollow tube, this comes out to be given by

$$J = \frac{\pi}{2}(r_o^4 - r_i^4), \tag{B8}$$

where r_o is the outer radius and r_i is the inner radius.

---

*Author to whom correspondence should be addressed. Electronic address: jindal@pu.ac.in

†Present address: Institute of Physikalische Chemie, University of Wuerzburg, Germany.

[1] "Physics News Update, The American Institute of Physics Bulletin of Physics News, Number 279 (Story No. 2)," July 15, 1996 by Phillip F. Schewe and Ben Stein ⟨http://www.aip.org/pnu/1996/split/pnu279-2.htm⟩

[2] M. M. J. Treacy, T. W. Ebbesen, and J. M. Gibson, Nature (London) **381**, 678 (1996).

[3] A. Krishnan, E. Dujardin, T. W. Ebbesen, P. N. Yianilos, and M. M. J. Treacy, Phys. Rev. B **58**, 14013 (1998).

[4] E. W. Wong, P. E. Sheehan, and C. M. Lieber, Science **277**, 1971 (1997).

[5] L. Forró, J.-P. Salvetat, J.-M. Bonard, R. Bacsa, N. H. Thomson, S. Garaj, L. Thien-Nga, R. Gaál, A. Kulik, B. Ruzicka, L. Degiorgi, A. Bachtold, C. Schönenberger, S. Pekker, and K. Hernadi, *Science and Application of Nanotubes*, edited by D. Tomànek and R. J. Enbody (Kluwer Academic/Plenum Publishers, New York, 2000), p. 297.

[6] G. Gao, T. Cagin, and W. A. Goddard III (1997), http://www.wag.caltech.edu/foresight/foresight_2.html

[7] E. Hernandez, C. Goze, P. Bernier, and A. Rubio, Phys. Rev. Lett. **80**, 4502 (1998).

[8] S. Tejima, Y. Miyamoto, K. Minami, M. Iizuka, and H. Nakamura, Annual Report of the Earth Simulator Center April 2003-March 2004, pp. 125–127.

[9] X. Zhou, J. Zhou, and Z. Ou-Yang, Phys. Rev. B **62**, 13692 (2000).

[10] A. Sears and R. C. Batra, Phys. Rev. B **69**, 235406 (2004).

[11] Y. Wang, X. X. Wang, and N. Xianggui, Modell. Simul. Mater. Sci. Eng. **12**, 1099 (2004).

[12] S. J. Papadakis, A. R. Hall, P. a. Williams, L. Vicci, M. R. Falvo, R. Superfine, and S. Washburn, Phys. Rev. Lett. **93**, 146101 (2004).

[13] V. N. Popov, V. E. VanDoren, and M. Balkanski, Phys. Rev. B **61**, 3078 (2000).

[14] J. P. Lu, Phys. Rev. Lett. **79**, 1297 (1997).

[15] D. W. Brenner, Phys. Rev. B **42**, 9458 (1990).

[16] J. Tersoff, Phys. Rev. B **37**, 6991 (1988); J. Tersoff, Phys. Rev. Lett. **61**, 2879 (1988).

[17] S. A. Chesnokov, V. A. Nalimova, A. G. Rinzler, R. E. Smalley, and J. E. Fischer, Phys. Rev. Lett. **82**, 343 (1999).

[18] U. D. Venkateswaran, A. M. Rao, E. Richter, M. Menon, A. Rinzler, R. E. Smalley, and P. C. Eklund, Phys. Rev. B **59**, 10928 (1999).

[19] M. J. Peters, L. E. McNeil, J. P. Lu, and D. Kahn, Phys. Rev. B **61**, 5939 (2000).

[20] J. Tang, L.-C. Qin, T. Sasaki, M. Yudasaka, A. Matsushita, and S. Iijima, Phys. Rev. Lett. **85**, 1887 (2000).

[21] M. J. Lopez, A. Rubio, J. A. Alonso, L.-C. Qin, and S. Iijima, Phys. Rev. Lett. **86**, 3056 (2001).

[22] S. Rols, I. N. Gontcharenko, R. Almairac, J. L. Sauvajol, and I. Mirebeau, Phys. Rev. B **64**, 153401 (2001).

[23] S. M. Sharma, S. Karmakar, S. K. Sikka, P. V. Teredesai, A. K. Sood, A. Govindaraj, and C. N. R. Rao, Phys. Rev. B **63**, 205417 (2001).

[24] S. Kumar, S. M. Sharma, P. V. Teredesai, D. V. S. Muthu, A. Govindaraj, S. K. Sikka, and A. K. Sood, New J. Phys. **5**, 143 (2003).

[25] G. B. Adams, O. F. Shankey, J. B. Page, M. O'Keefe, and D. A. Drabold, Science **256**, 1792 (1992).

[26] B. I. Yakobson, C. J. Brabec, and J. Bernholc, Phys. Rev. Lett. **76**, 2511 (1996).

[27] M. S. Dresselhaus, G. Dresselhaus, and P. C. Eklund, *Science of Fullerenes and Carbon Nanotubes* (Academic, New York, 1996).

[28] D. Sanchez-Portal, E. Artacho, J. M. Soler, A. Rubio, and P. Ordejon, Phys. Rev. B **59**, 12678 (1999).

[29] O. L. Blaskslee, D. G. Proctor, E. J. Seldin, G. B. Spence, and T. Weng, J. Appl. Phys. **41**, 3373 (1970).

[30] A. I. Kitaigorodski, *Molecular Crystals and Molecules* (Academic, New York, 1973).

[31] V. K. Jindal, K. Dharamvir, and S. Singh, Int. J. Mod. Phys. B **14**, 51 (2000).

[32] R. Kumar, K. Dharamvir, and V. K. Jindal, Physica B **365**, 121 (2005).

[33] J. Tersoff and R. S. Ruoff, Phys. Rev. Lett. **73**, 676 (1994).

[34] G. Sun, J. Kürti, M. Kertesz, and R. H. Baughman, J. Phys. Chem. B **107**, 6924 (2003).